Revista Brasileira de Física, Vol. 4, N.º 2, 1974

Coexistence of Two-Neutron-Hole and Vibrational Degrees of Freedom: ^{94}Mo as an Example

V. PAAR,
The Niels Bohr Institute, University of Copenhagen, Copenhagen, Denmark
and
Institute Rudjer Bŏsković, Zagreb, Yugoslavia[1]

Recebido em 2 de Fevereiro de 1974

The properties of the ^{94}Mo nucleus, which is a typical representative of N = 52 nuclei, have been calculated in the cluster-field model in natural representation (without parameter fitting). The competition between two-neutron valence-shell and vibrational degrees of freedom, giving rise to the coexistence of quasivibrational, quasirotational, and clustering phenomena has been demonstrated and conceptual problems have been discussed.

São calculadas as propriedades do núcleo de ^{94}Mo, um representante típico de nucleos com N igual a 52, no modelo de *cluster-field* e na representação natural (sem ajuste de parâmetros). Demonstra-se a competição entre os graus de liberdade vibracionais e dos dois neutrons de valência, competição essa que dá origem à coexistência de fenômenos quasi-vibracionais, quasi-rotacionais e de *clustering* e discutem-se problemas conceituais.

1. Introduction

Experimental studies of $^{94}_{42}Mo_{52}$ have been performed by Coulomb excitation [1-3], decay experiments[4-7] and by the reactions ^{94}Mo (d, d') [Ref. 8], ^{94}Mo (p, p') [Ref. 9], ^{94}Mo (d, n)^{95} Tc [Ref. 10], ^{92}Zr (α, 2nγ) ^{94}Mo [Refs. 11,121, ^{94}Mo (p, d) ^{93}Mo [Ref. 131, ^{94}Mo (d, t) ^{93}Mo [Refs. 14,151, ^{94}Mo (p, t) ^{92}Mo [Refs. 16,171, ^{93}Nb (^{3}He, d) ^{94}Mo [Ref. 18] and ^{95}Mo (d, t) ^{94}Mo [Ref. 19].

In theoretical considerations, ^{94}Mo has been described by shell-model calculations using the effective interaction method with a rather restricted configuration space[22,23]. This nucleus has also been discussed in the framework of the collective asyrnmetric rotor model[7,26].

The present description is based on coupling single-particle to collective degrees of freedom.

[1] Permanent address.

The ^{94}Mo nucleus has two neutrons outside the N = 50 closed shell, while the 28-50 proton shell is open. On the other hand, the neutron closed-shell ^{92}Mo nucleus exhibits a pronounced low-frequency quadrupole mode (the B(E2) value is $\approx$ 10 s.p.u.). Therefore, the properties of the N = 52 system are expected to be given by an interplay of two-neutron valence-shell single-particle and collective degrees of freedom. The mechanism of the particle (or quasiparticle)-vibration coupling generally appears to play an important role in creating the properties of spherical transitional nuclei[24-46,48-51].

An analogous description has been successfully performed for the corresponding nuclei having two proton particles (even Te[33,38,39,40]) and holes (even Hg[32,33,35,39]) in the 50-82 proton shells, with neutron shells being open.

The ^{95}Mo nucleus, having three neutrons outside the N = 50 closed shell, has been successfully described within the same natural parametrization as used here for ^{94}Mo, by coupling three valence-shell neutrons to the vibration[57].

The effects of coupling a three-particle (hole) cluster to the vibrational field have also been successfully studied in the 50-82 proton shell[32,33,41,45,57].

2. Difficulties Facing the Shell-Model Approach

Although available shell-model calculations[22-24,12] account satisfactorily for a number of properties of ^{94}Mo, they are in disagreement with a few pronounced experimental facts:

(i) The quasivibrational pattern of the electromagnetic properties of low-lying states. The experimental B(E2) values for the $2_1^+ \rightarrow 0_1^+$, $2_1^+ \rightarrow 2_1^+$, and $4_1^+ \rightarrow 2_1^+$ stop-over transitions are strongly enhanced over the single-particle estimate, while the $2_2^+ \rightarrow 0_1^+$ crossover transition is reduced by almost two orders of magnitude relative to strong stopover transitions. The results obtained by the shell-model calculation[23] using the effective charges $e^p_{eff} = 1.71$ and $e^n_{eff} = 1.81$ are compared with experimental data in Table I. The B(E2) value for the shell-model crossover transition calculated in Ref. 23 is larger than the one for the $2_2^+ \rightarrow 2_1^+$ stopover transition, in contradiction to experiment;

	Experiment[a]	Experiment[b]	Shell model[c]	Present model
B(E2) $(2_1 \rightarrow 0_1)$ $(eb)^2$	0.054 ± 0.008	0.044 ± 0.002	0.037	0.050
B(E2) $(2_2 \rightarrow 0_1)$ $(eb)^2$	0.0011 ± 0.0003	0.0006 ± 0.0001	0.0046	0.001
B(E2) $(2_2 \rightarrow 2_1)$ $(eb)^2$	0.031	0.116 ± 0.026	0.0035	0.033
B(E2) $(4, \rightarrow 2_1)$ $(eb)^2$	large	0.067 ± 0.010		0.057
B(M1) $(2_2 \rightarrow 2_1)$ $(\mu_N)^2$	0.235	0.020 ± 0.007	3.76	0.041

a) Ref. 1; b) Ref. 58; c) Ref. 15.

Table I. Comparison of the B(E2) and B(M1) values available from experiment, results of of the shell-model calculations, and results of the present calculation.

(ii) Relative spectroscopic strengths to the first and second 2^+ state in the ^{93}Nb(^{3}He, d) ^{94}Mo stripping reaction. It has been experimentally observed that the first 2^+ state is more strongly excited than the second 2^+ state by one order of magnitude. The prediction of the existing shell-model calculation[23] is in disagreement with this experimental fact. The 2_2^+ state in the shell-model calculation[23] is predicted to be more strongly excited than the 2_1^+ state, because the corresponding calculated states derive most of their parentage from the $(1g_{9/2})^2 2$ proton and $(2d_{5/2})^2 2$ neutron group, respectively. The coupling of a transferred $g_{9/2}$ proton with an unpaired $g_{9/2}$ proton in the ground state of ^{93}Nb should then preferentially excite the second 2^+ rather than the first 2^+ state in ^{94}Mo;

(iii) The presence of a noticeable amount of transfer strength to the $2d_{3/2}$, $3s_{1/2}$, $1h_{11/2}$, and $1g_{7/2}$ neutron orbitals[14,21] and to the $2p_{3/2}$ and $1f_{5/2}$ proton orbitals[18] in the low-lying part of the spectrum. These configurations have been neglected in the shell-model calculations performed so far.

(iv) It should also be stressed that several observed low-lying states in ^{95}Mo are not reproduced in the restricted shell-model calculations[22,23]. This indicates the presence of collective modes which give rise to a multiplet pattern.

3. The Present Model

The Harniltonian of the nuclear system is[27,30,33]

$$H = H_{\mathrm{SH}} + H_{\mathrm{VIB}} + H_{\mathrm{RES}} + k \sum_{i=1}^{2} \sum_{\mu} \alpha_2^{\mu} \, Y_2^{\mu *} (\theta_i, \phi_i).$$

Here H_{SH} describes the motion of two valence-shell particles (holes) in the shell-model potential, and H_{VIB} represents the free quadrupole vibrational field. The residual interaction H_{RES} explicitly includes only the pairing force[33].

The bare particle-field coupling strength is defined by

$$a = \frac{1}{(4\pi)^{1/2}} \langle k \rangle \left(\frac{\hbar\omega_2}{2c_2} \right)^{1/2}$$

The Q−Q component of the residual force as well as high-frequency quadrupole modes and the isovector potential are included in the renormalization of the bare particle-field coupling strength[28,41,42]. In the present case, the effects of the isovector potential arid of the bare Q−Q force act in opposite directions.

The Harniltonian is diagonalized in the basis built from $|(l_1 j_1, l_2 j_2)\mathrm{J}, \mathrm{NR}; \mathrm{I}\rangle$ states. Here N and R represent the number of phonons and the angular momentum of the N-phonon state, respectively.

The electric quadrupole and magnetic dipole operators consist of a particle (hole) and a vibrational part[27,33]

$$M^{\mu}(\mathrm{E2}) = \sum_{i=1}^{2} e^{\mathrm{s.p.}}\, r_i^2\, Y_2^{\mu}(\theta_i, \phi_i) + \frac{3}{4\pi}\, e^{\mathrm{vib}}\, R_0^2\, (b_2^{\mu\dagger} + (-)^{\mu}\, b_2^{-\mu}),$$

$$\mathbf{M}(\mathrm{M1}) = \left(\frac{3}{4\pi}\right)^{1/2} |g_{\mathrm{R}}\mathrm{I} + (g_l - g_{\mathrm{R}})\mathrm{J} + (g_s - g_l)\mathrm{S}|\mu_{\mathrm{N}}.$$

Here all notation has the usual meaning. I is the total angular momentum of the nucleus, and J and S are the total angular rnomentum operator and the spin of the two-particle valence-shell state, respectively.

The matrix elements of the electric quadrupole and magnetic dipole operators are expressed in the forms[33]

$$\langle \mathrm{I_k} \,\|\, \mathrm{M(E2)} \,\|\, \mathrm{I_k'} \rangle = (e^{\mathrm{s.p.}}\, A + e^{\mathrm{vib}}\, B)\, R_0^2\ \mathrm{e.b},$$
$$\langle \mathrm{I_k} \,\|\, \mathrm{M(M1)} \,\|\, \mathrm{I_k'} \rangle = (g_R C + g_l D + g_s E)\, \mu_N.$$

Here the quantities A, B, C, D, and E are calculated from the model wave functions, $e^{\mathrm{s.p.}}$ and e^{vib} are the effective single-particle and vibrator charge,

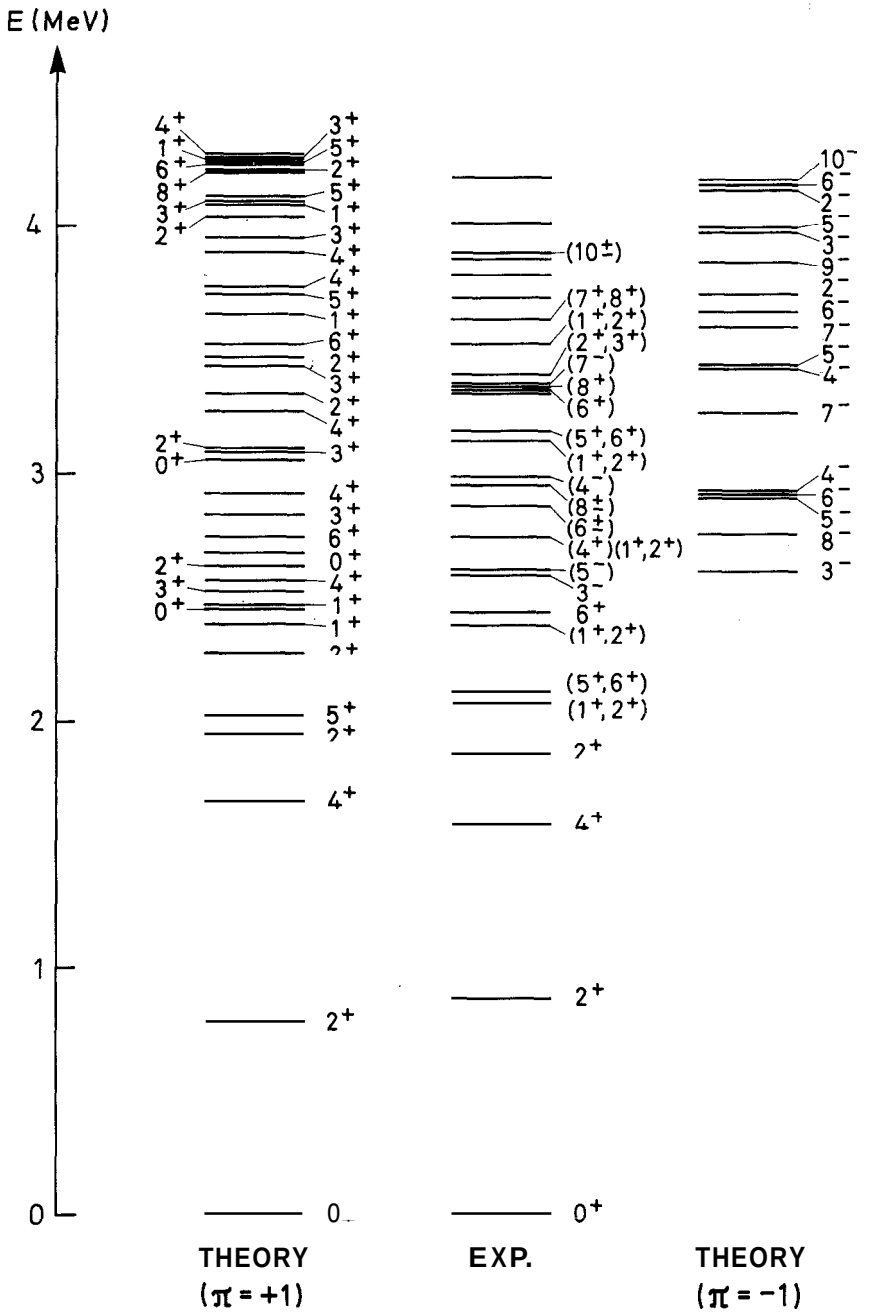

Fig. 1 - Calculated and experimental levels of ^{94}Mo.

0_1^+

$\|(d_{5/2})^2 0,00\rangle$	−0.619
$\|(s_{1/2})^2 0,00\rangle$	−0.222
$\|(g_{7/2})^2 0,00\rangle$	−0.252
$\|(d_{3/2})^2 0,00\rangle$	−0.206
$\|(h_{11/2})^2 0,00\rangle$	0.210
$\|(d_{5/2})^2 0,20\rangle$	−0.185
$\|(d_{5/2})^2 2,12\rangle$	0.335
$\|(d_{5/2}s_{1/2})2,12\rangle$	0.301
$\|(d_{5/2}d_{3/2})2,12\rangle$	0.118
$\|(s_{1/2}d_{3/2})2,12\rangle$	0.139
$\|(g_{7/2}d_{3/2})2,12\rangle$	0.124
$\|(d_{5/2}s_{1/2})2,22\rangle$	−0.146
$\|(d_{5/2})^2 4,24\rangle$	−0.131
$\|(d_{5/2}d_{3/2})4,24\rangle$	0.129

2_1^+

$\|(d_{5/2})^2 0,12\rangle$	−0.521
$\|(s_{1/2})^2 0,12\rangle$	−0.209
$\|(g_{7/2})^2 0,12\rangle$	−0.189
$\|(d_{3/2})^2 0,12\rangle$	−0.168
$\|(h_{11/2})^2 0,12\rangle$	0.149
$\|(d_{5/2})^2 0,22\rangle$	0.106
$\|(d_{5/2})^2 2,00\rangle$	0.294
$\|(d_{5/2}s_{1/2})2,00\rangle$	0.244

2_1^+ (continued)

$\|(s_{1/2}d_{3/2})2,00\rangle$	0.108
$\|(d_{5/2}s_{1/2})2,12$	−0.209
$\|(d_{5/2})^2 2,20\rangle$	0.128
$\|(d_{5/2}s_{1/2})2,20\rangle$	0.127
$\|(d_{5/2})^2 2,22\rangle$	0.141
$\|(d_{5/2}s_{1/2})2,22\rangle$	0.125
$\|(d_{5/2})^2 2,24\rangle$	0.201
$\|(d_{5/2}s_{1/2})2,24\rangle$	0.188
$\|(d_{5/2})^2 4,12\rangle$	−0.184
$\|(d_{5/2}d_{3/2})4,12\rangle$	−0.162

4_1^+

$\|(d_{5/2})^2 0,24\rangle$	0.314
$\|(s_{1/2})^2 0,24\rangle$	0.134
$\|(d_{5/2})^2 2,12\rangle$	−0.325
$\|(d_{5/2}s_{1/2})2,12\rangle$	−0.299
$\|(s_{1/2}d_{3/2})2,12\rangle$	−0.140
$\|(d_{5/2}s_{1/2})2,22\rangle$	0.116
$\|(d_{5/2}s_{1/2})2,24\rangle$	0.179
$\|d_{5/2})^2 4,00\rangle$	0.391
$\|(d_{5/2}g_{7/2})4,00\rangle$	0.102
$\|d_{5/2}d_{3/2})4,00\rangle$	0.253
$\|(s_{1/2}g_{7/2})4,00\rangle$	0.115
$\|(d_{5/2})^2 4,12\rangle$	−0.191

4_1^+ (continued)

$\|(d_{5/2}d_{3/2})4,12\rangle$	−0.217
$\|(d_{5/2})^2 4,20\rangle$	0.137
$\|(d_{5/2}d_{3/2})4,20\rangle$	0.129
$\|(d_{5/2})^2 4,22\rangle$	0.100
$\|(d_{5/2}d_{3/2})4,24\rangle$	0.126
$\|(d_{5/2}g_{7/2})6,12\rangle$	−0.210
$\|(d_{5/2}g_{7/2})6,22\rangle$	0.102

2_2^+

$\|(d_{5/2})^2 0,12\rangle$	0.173
$\|(d_{5/2})^2 0,22\rangle$	0.320
$\|(d_{5/2})^2 2,00\rangle$	−0.385
$\|(d_{5/2}s_{1/2})2,00\rangle$	0.224
$\|(d_{5/2}g_{7/2})2,00\rangle$	−0.108
$\|(d_{5/2}d_{3/2})2,00\rangle$	0.203
$\|(d_{5/2})^2 2,12\rangle$	−0.464
$\|(d_{5/2}g_{7/2})2,12\rangle$	−0.151
$\|(s_{1/2}d_{3/2})2,12\rangle$	−0.118
$\|(d_{5/2})^2 2,20\rangle$	−0.108
$\|(d_{5/2}s_{1/2})2,20\rangle$	0.109
$\|(d_{5/2}d_{3/2})2,20\rangle$	0.100
$\|(d_{5/2})^2 2,32\rangle$	−0.108
$\|(d_{5/2}s_{1/2}3,12\rangle$	0.176
$\|(\quad)2,12\rangle$	0.108

2_2^+ (continued)

$\|(d_{5/2}d_{3/2})3,12\rangle$	0.147
$\|(d_{5/2}d_{3/2})4,12\rangle$	−0.147
$\|(d_{5/2})^2 4,24\rangle$	0.214

2_3^+

$\|(d_{5/2})^2 0,12\rangle$	0.264
$\|(g_{7/2})^2 0,12\rangle$	0.174
$\|(d_{3/2})^2 0,12\rangle$	0.137
$\|(h_{11/2})^2 0,12\rangle$	−0.118
$\|(d_{5/2})^2 0,22\rangle$	0.179
$\|(d_{5/2}g_{7/2})1,12\rangle$	−0.165
$\|(d_{5/2}d_{3/2})1,12\rangle$	0.236
$\|(d_{5/2})^2 2,00\rangle$	0.367
$\|(d_{5/2}s_{1/2})2,00\rangle$	0.163
$\|(d_{5/2}g_{7/2})2,00\rangle$	−0.207
$\|(d_{5/2}d_{3/2})2,00\rangle$	−0.263
$\|(d_{5/2})^2 2,12\rangle$	−0.109
$\|(d_{5/2}s_{1/2})2,12\rangle$	−0.216
$\|(d_{5/2}d_{3/2})2,20\rangle$	−0.112
$\|(d_{5/2})^2 2,24\rangle$	−0.149
$\|(d_{5/2}s_{1/2})3,12\rangle$	−0.126
$\|(d_{5/2}s_{1/2})3,22\rangle$	0.108
$\|(d_{5/2})^2 4,12\rangle$	−0.362

2_3^+ (continued)

$\|(d_{5/2}g_{7/2})4,12\rangle$	0.125
$\|(d_{5/2})^2 4,22\rangle$	0.151

5_1^+

$\|(d_{5/2}g_{7/2})1,24\rangle$	0.128
$\|(d_{5/2}d_{3/2})1,24\rangle$	0.129
$\|(d_{5/2})^2 2,24\rangle$	−0.182
$\|(d_{5/2}d_{3/2})2,24\rangle$	0.160
$\|(d_{5/2}g_{7/2})3,12\rangle$	−0.309
$\|(d_{5/2}d_{3/2})3,12\rangle$	−0.316
$\|(s_{1/2}g_{7/2})3,12\rangle$	−0.112
$\|(d_{5/2}s_{1/2})3,24\rangle$	−0.153
$\|(d_{5/2})^2 4,12\rangle$	0.319
$\|(d_{5/2}d_{3/2})4,12\rangle$	−0.145
$\|(s_{1/2}g_{7/2})4,12\rangle$	0.140
$\|(d_{5/2})^2 4,24\rangle$	−0.124
$\|(d_{5/2}g_{7/2})5,00\rangle$	0.555
$\|(d_{5/2}g_{7/2})5,12\rangle$	−0.213
$\|(d_{5/2}g_{7/2})5,20\rangle$	0.162
$\|(d_{5/2}g_{7/2})5,22\rangle$	0.104

1_1^+

$\|(d_{5/2}g_{7/2})1,00\rangle$	0.328

1_1^+ (continued)

$\|(d_{5/2}d_{3/2})1,00\rangle$	−0.387
$\|(s_{1/2}d_{3/2})1,00\rangle$	0.140
$\|(d_{5/2}g_{7/2})1,20\rangle$	0.133
$\|(d_{5/2}d_{3/2})1,20\rangle$	−0.176
$\|(d_{5/2}g_{7/2})1,22\rangle$	−0.115
$\|(d_{5/2}d_{3/2})1,22\rangle$	0.145
$\|(d_{5/2})^2 2,12\rangle$	0.274
$\|(d_{5/2}s_{1/2})2,12\rangle$	0.117
$\|(d_{5/2}g_{7/2})2,12\rangle$	−0.352
$\|(d_{5/2}d_{3/2})2,12\rangle$	−0.351
$\|(d_{5/2}s_{1/2})3,12\rangle$	−0.175
$\|(d_{5/2}d_{3/2})3,12\rangle$	0.102
$\|(s_{1/2}g_{7/2})3,12\rangle$	−0.148
$\|(d_{5/2}s_{1/2})3,22\rangle$	0.119
$\|(d_{5/2})^2 4,24\rangle$	−0.253
$\|(d_{5/2}g_{7/2})4,24\rangle$	0.161

0_2^+

$\|(d_{5/2})^2 0,00\rangle$	0.208
$\|(g_{7/2})^2 0,00\rangle$	0.407
$\|(d_{3/2})^2 0,00\rangle$	0.263
$\|(h_{11/2})^2 0,00\rangle$	−0.266
$\|(d_{5/2})^2 0,20\rangle$	−0.367
$\|s_{1/2})^2 0,20\rangle$	−0.139

0_2^+ (continued)

$\|(d_{5/2})^2 2,12\rangle$	0.264
$\|(d_{5/2}s_{1/2})2,12\rangle$	0.278
$\|(g_{7/2})^2 2,12\rangle$	−0.160
$\|(g_{7/2}d_{3/2})2,12\rangle$	−0.203
$\|(d_{5/2})^2 2,22\rangle$	−0.103
$\|(d_{5/2}s_{1/2})2,22\rangle$	−0.222
$\|(d_{5/2})^2 2,32\rangle$	0.194
$\|(d_{5/2}s_{1/2}2,32\rangle$	0.183
$\|(d_{5/2})^2 4,24\rangle$	−0.270
$\|(d_{5/2}d_{3/2})4,24\rangle$	−0.126

6_1^+

$\|(d_{5/2})^2 0,36\rangle$	0.100
$\|(d_{5/2})^2 2,24\rangle$	−0.191
$\|(d_{5/2}s_{1/2})2,24\rangle$	−0.187
$\|(s_{1/2}d_{3/2})2,24\rangle$	−0.108
$\|(d_{5/2})^2 4,12\rangle$	0.304
$\|(d_{5/2}g_{7/2})4,12\rangle$	0.144
$\|(d_{5/2}d_{3/2})4,12\rangle$	0.336
$\|(s_{1/2}g_{7/2})4,12\rangle$	0.184
$\|(d_{5/2})^2 4,22\rangle$	−0.104
$\|(d_{5/2}d_{3/2})4,22\rangle$	−0.162
$\|(d_{5/2})^2 4,24\rangle$	−0.120
$\|(d_{5/2}d_{3/2})4,24\rangle$	−0.183

6_1^+ (continued)

$\|(d_{5/2}g_{7/2})6,00\rangle$	−0.492
$\|(d_{5/2}g_{7/2})6,12\rangle$	0.376
$\|(d_{5/2}g_{7/2})6,20\rangle$	−0.188
$\|(d_{5/2}g_{7/2})6,24\rangle$	−0.181

8_1^+

$\|(d_{5/2})^2 2,36\rangle$	0.121
$\|(d_{5/2}s_{1/2})2,36\rangle$	0.143
$\|(d_{5/2})^2 4,24\rangle$	−0.295
$\|(d_{5/2}g_{7/2})4,24\rangle$	−0.161
$\|(d_{5/2}d_{3/2})4,24\rangle$	−0.361
$\|(s_{1/2}g_{7/2})4,24\rangle$	−0.179
$\|(d_{5/2}d_{3/2})4,34\rangle$	0.144
$\|(d_{5/2}d_{3/2})4,36\rangle$	0.144
$\|(d_{5/2}g_{7/2})6,12\rangle$	0.640
$\|(d_{5/2}g_{7/2})6,22\rangle$	−0.240
$\|(d_{5/2}g_{7/2})6,24\rangle$	−0.326
$\|(d_{5/2}g_{7/2})6,32\rangle$	0.148
$\|(d_{5/2}g_{7/2})6,36\rangle$	0.132

Table II - Wave functions of a few low-lying positive-parity states in ^{94}Mo. Only those amplitudes which are larger than $1^0/_0$ are listed.

respectively. The nuclear radius $R_i = 0.12\ A^{1/3} \times 10^{-12} cm$ is used. The quantities g_R, g_l, and g_s are the gyromagnetic ratios.

The bare charges and the gyromagnetic ratios for neutrons are $e^{s.p.} = 0$, $e^{vib} = Z\left(\frac{\hbar\omega_2}{2c_2}\right)^{1/2}_{vib}$, $g_R = Z/A$, $g_l = 0$, and $g_s = -3.82$.

Details of the present model are given in Refs. 32 and 33.

4. Results of the Calculation

The present approach is based on the assumption that $^{92}_{42}Mo_{50}$ plays the role of a basic vibrational field to which a two-neutron valence-shell cluster is coupled. The basic arguments are as follows: (i) $B(E2)$ $(2_1 \rightarrow 0_1)$ in ^{92}Mo is appreciably enhanced over the single-particle estimate; (ii) $N = 50$ is a rather good closed shell.

In the present calculation we use the single-particle levels determined by the $^{92}Mo(d, p)\ ^{93}Mo$ reaction in Ref. 21, i.e.,

$$\begin{aligned} &\varepsilon(s_{1/2}) - \varepsilon(d_{5/2}) = 1.55 \text{ Mev}, \\ &\varepsilon(g_{7/2}) - \varepsilon(d_{5/2}) = 1.50 \text{ MeV}, \\ &\varepsilon(d_{3/2}) - \varepsilon(d_{5/2}) = 1.89 \text{ MeV}, \\ &\varepsilon(h_{11/2}) - \varepsilon(d_{5/2}) = 2.22 \text{ MeV}. \end{aligned}$$

The experimental phonon energy is takeri from ^{92}Mo (bare value)

$$\hbar\omega_2 = 1.51 \text{ MeV}.$$

The value for the effective pairing strength

$$G = 0.25$$

was estimated in 'the usual way[46].

In the Bohr-Mottelson approach, the base particle-vibration coupling is given by[27,28]

$$a_{BM} = \frac{(4\pi)^{1/2}}{3ZeR_0^2}\ (k)\ \left|\langle B^{vib}(E2,\ 2_1 \rightarrow 0_1)\rangle\right|^{1/2}.$$

The radial matrix element (k) is estimated to be 50 MeV [Ref. 28], while the $B^{vib}(E2,\ 2_1 \rightarrow 0_1)$ value has to be taken from the nucleus vibrator

(^{92}Mo) [Ref. 28]. This gives the estimate

$$a_n \approx (0.73 \pm 0.06)\ \text{MeV}.$$

In the present calculation we use the particle-field coupling strenght $a = 0.8$. This value gives over-all agreement with experirnent.

The calculated and experimental levels are compared in Fig. 1. The truncation of a phonon space results generally in the stretching of the theoretical spectrum[41]. The wave functions for a few low-lying positive-parity states are listed in Table II. The ground and first excited state are based on the $|(d_{5/2})^2 0,00;0\rangle$ and $|(d_{5/2})^2 0,12;2\rangle$ components, respectively. However, admixtures to these components are rather large, especially those configurations coming from the $\Delta N = 1$ nonspin-flip processes, such as $|(d_{5/2})^2 2,12;0\rangle$ and $|(d_{5/2}s_{1/2})2,12;0\rangle$ to the first component and $|(d_{5/2})^2 2,00;2\rangle$ and $|(d_{5/2}s_{1/2})2,00;2\rangle$ to the second component.

The static electric quadrupole and magnetic dipole moments are given in Table III. Tables IV and V list the calculated B(E2) and B(M1) values,

						Q (eb)		μ (μ_N)	
	A	*B*	**C**	**D**	**E**	I	II	I'	11'
2_1	–0.461	–0.409	1.661	0.970	0.045	–0.27	–0.29	0.39	0.42
4_1	–0.700	–0.629	2.365	3.974	0.217	–0.41	–0.45	0.10	0.21
2_2	0.344	0.444	0.982	1.118	0.577	0.29	0.30	–1.34	–0.99
2_3	0.025	–0.050	0.815	1.411	0.451	–0.03	–0.03	–1.03	–0.76
5_1	–0.411	–0.452	2.599	6.006	0.271	–0.28	–0.30	0.03	0.16
1_1	0.132	0.140	0.318	0.805	0.074	0.07	0.07	–0.12	–0.07
4_2	–0.441	–0.446	1.224	4.078	1.253	–0.29	–0.31	–2.61	–1.98
6_1	–0.979	–0.963	2.926	8.325	0.166	–0.58	–0.62	0.31	0.39
6_2	–0.485	–0.541	4.560	5.637	1.219	–0.33	–0.34	–1.44	–0.92
8_1	–1.095	–0.832	6.400	10.505	0.190	–0.46	–0.52	0.92	0.99
8_2	–0.478	–0.325	9.054	6,378	1.662	–0.18	–0.21	–1.19	–0.55
10_1	–1.195	–0.592	10.499	12.789	0.195	–0.31	–0.38	1.56	1.63
10_2	–0.432	–0.023	13.995	7.496	1.992	–0.01	–0.05	–0.74	–0.04

Table III. Static electric quadrupole and magnetic dipole moments of low-lying positive-parity states in ^{94}Mo.

The quantities *A*,*B*,*C*,*D*, and E, defined in Sec. III, are calculated from the model wave functions. The static quadrupole moments Q (eb) are given for two choices of the effective charges (I) e'' = Q e^{vib} = 2.9 (bare values) and (II) e'' = 0.5, e^{vib} = 2.6.

The magnetic dipole moments $\mu(\mu_N)$ are given for the following two choices of the effective gyromagnetic ratios (I') $g_R = Z/A$, $g_l = 0$, $g_s = g_s^{free}$ (n) (bare values) and (II') $g_R = Z/A$, $g_l = 0$, $g_s = 0.8\ g_s^{free}$ (n).

respectively, for transitions between low-lying positive-parity states and for transitions in the yrast region. The calculation reproduces large "stopover" and small "crossover" transitions in the low-lying part of the spectrum, and gives strong $\ldots 10_1^+ \to 8_1^+ \to 6_1^+ \to 4_1^+ \to 2_1^+ \to 0_1^+$ E2 transitions inside the ground-state "quasirotati~snaband".

The calculated low-lying negative-parity states are also shown in Fig. I, and the dominant components in the wave functioris for these states are listed in Table VI.

5. Coexistence of the Quasivibrational and Quasirotational Structures

The speciiic general pattern produced by the cluster-field mechanism is the coexistence of quasivibrational arid quasirotational characteristics[39,41]. In the present paper we study these properties in the case of ^{94}Mo. The quasivibrational situation, with strong stopover and small crossover transitions, is generally reestablished in the cluster-field system[39]. The theoretical $0_2^+ \to 2_1^+$, $2_2^+ \to 2_1^+$, and $4_1^+ \to 2_1^+$ transitions are strong, while the $2_2^+ \to 0_1^+$ crossover transition is appreciably weaker. The experimental $2_2^+ \to 2_1^+$, $4_1^+ \to 2_1^+$, and $2_2^+ \to 0_1^+$ transitions in ^{94}Mo reveal the same quasivibrational characteristics. It would be interesting to locate the 0_2^+ state [earlier (p,p′) experiments indicate that the 2.066-MeV state is a possible candidate] and to measure the $\bar{B}$(E2) value for the $0_2^+ \to 2_1^+$ transition. Although the quasivibrational situation is established, the 0_2^+, 2_2^+, and 4_1^+ model states are not based on two-phonon excitations, as supposed in the pure vibrational picture, but are of a rather mixed character, arising from zero-, one-, and zero-phonon states, respectively, as seen from Table II. Stopover transitions are generally enhanced, because of the coherence of the single-particle arid vibrational contributions to transition moments [generalized vibrational selection and intensity rules, GVISR[39]]. Furthermore, the 0_2^+, 2_2^+, and 4_1^+ model states, which resemble vibrational "triplet" states, may lie rather far apart from each other, since they are of different character, already in zeroth order. Some other states, therefore, can also appear in this energy region. In the case of ^{94}Mo, the 0_2^+ state is systematically pushed up in natural representation. This fact should be particularly emphasized, because it is sometimes used as an argument against the presence of modes of the vibrational type.

The reduction of the crossover transition is a consequence of the incoherence of single-particle and collective contributions to the corresponding

			B(E2) (eb)^2					B(E2) (eb)^2	
	A	B	I	II		A	B	I	II
$2_1 \rightarrow 0_1$	0.441	0.581	0.050	0.053	$6_1 \rightarrow 5_1$	−0.059	−0.062	0.000	0.000
$2_2 \rightarrow 0_1$	0.051	−0.079	0.001	0.001	$6_2 \rightarrow 6_1$	−0.174	−0.293	0.005	0.005
$2_3 \rightarrow 0_1$	0.095	−0.182	0.005	0.003	$6_2 \rightarrow 4_1$	−0.156	−0.598	0.021	0.018
$4_1 \rightarrow 2_1$	−0.759	−0.826	0.057	0.063	$6_1 \rightarrow 4_2$	0.351	0.229	0.003	0.004
$2_2 \rightarrow 2_1$	−0.351	−0.473	0.033	0.035	$6_2 \rightarrow 4_2$	0.446	0.829	0.039	0.039
$2_3 \rightarrow 2_1$	−0.108	−0.235	0.008	0.008	$8_1 \rightarrow 6_1$	−0.798	−1.305	0.075	0.075
$1_1 \rightarrow 2_1$	−0.003	0.047	0.001	0.000	$8_1 \rightarrow 6_2$	0.151	0.009	0.000	0.000
$0_2 \rightarrow 2_1$	0.122	0.188	0.026	0.027	$8_2 \rightarrow 6_1$	−0.006	0.207	0.002	0.002
$2_2 \rightarrow 4_1$	−0.105	−0.019	0.000	0.000	$8_2 \rightarrow 6_2$	−0.527	−1.389	0.085	0.078
$5_1 \rightarrow 4_1$	−0.005	−0.156	0.002	0.001	$8_2 \rightarrow 8_1$	−0.132	−0.223	0.002	0.002
$2_3 \rightarrow 4_1$	−0.085	−0.197	0.006	0.005	$10_1 \rightarrow 8_1$	−0.718	−1.560	0.086	0.082
$4_2 \rightarrow 4_1$	−0.238	−0.176	0.003	0.003	$10_1 \rightarrow 8_2$	0.052	−0.260	0.002	0.002
$6_1 \rightarrow 4_1$	0.866	0.945	0.051	0.057	$10_2 \rightarrow 8_1$	−0.069	−0.279	0.003	0.002
$2_3 \rightarrow 2_2$	0.019	−0.042	0.000	0.000	$10_2 \rightarrow 8_2$	0.490	1.584	0.089	0.080
$1_1 \rightarrow 2_2$	−0.092	−0.121	0.004	0.004	$10_2 \rightarrow 10_1$	0.026	0.124	0.001	0.001
$0_2 \rightarrow 2_2$	0.037	0.009	0.000	0.000					

Table IV - Calculated E2 transitions in the low-lying part of the positive-parity spectrum and in the yrast region. For description see Table III.

				B(M1) $(\mu_N)^2$	
	C	D	E	I′	II′
$2_2 \rightarrow 2_1$	−0.113	0.244	−0.131	0.04	0.02
$2_3 \rightarrow 2_1$	−0.829	0.621	0.208	0.26	0.19
$1_1 \rightarrow 2_1$	−0.063	0.139	−0.076	0.02	0.01
$5_1 \rightarrow 4_1$	−0.108	0.216	−0.108	0.01	0.01
$2_3 \rightarrow 2_2$	0.511	0.020	−0.530	1.00	0.65
$6_1 \rightarrow 5_1$	0.344	−0.573	0.229	0.05	0.03
$4_2 \rightarrow 4_1$	0.008	0.461	−0.470	0.36	0.22
$6_2 \rightarrow 6_1$	−1.659	1.844	−0.185	0.00	0.00
$8_2 \rightarrow 8_1$	−1.217	1.398	−0.182	0.00	0.00
$10_2 \rightarrow 10_1$	0.552	−0.509	−0.043	0.01	0.01

Table V - Calculated M1 transitions in the low-lying part of the positive-parity spectrum and in the yrast region. For description see Table III.

B(E2) value[39]. The ground state is based on the $(d_{5/2})^2 0$ pair, while the basic state for the second 2^+ state is the $|(d_{5/2})^2 2,12;2\rangle$ one-phonon broken-pair state. In this case, lowest-order processes contributing to the B(E2) value for the crossover transition are represented by first-order particle and second-order induced collective diagrams in Fig. 2. To each single-particle diagram drawn on the left-hand side correspond three induced collective diagrarns drawn on the right-harid side, with all possible time-orderings of the emission or absorption of the virtual phonon. These induced second-order diagrams give rise to a factorization of energy denominators into two factors. The first factor corresponds to a first-order parent particle diagram and the second to the induced collective contribution. The second factor involves in the denominators the difference between the initial- and final-state energies $(-\mathrm{A}-\hbar\omega)$ addeú to and subtracted from the phonon energy

$$(\hbar\omega)\left[\left(-\frac{1}{\Delta+2\hbar\omega}+\frac{1}{\Delta}\right)\text{ for each line in Fig. 2}\right],$$

thus expressing an "on-energy-shell" effect. Here A is the pairing gap. The topological structure of the first-order parent particle diagram corresponds to those of the induced collective processes and, therefore, the kinematical structure[given by the corresponding JBV diagrams[43]] and the rest of dynamical structure are identical. Thus, the induced collective diagrams lead only to a renormalization of the single-particle effective charge. The factoriza-

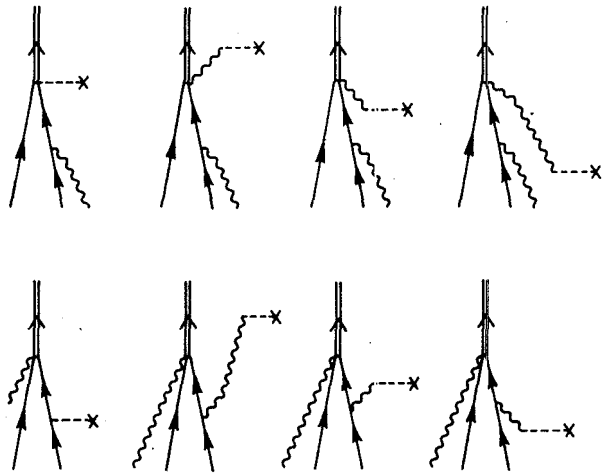

Fig. 2 - First-order particle and second-order induced collective diagrams representing leading-order processes for the $2_2^+ \rightarrow 0_1^+$ crossover transition in ^{94}Mo in natural representation. Particle diagrams involve the electromagnetic field interacting with single-particle states.

3_1^-		6_1^-	
$\|(d_{5/2}h_{11/2})\ 3,00\rangle$	0.631	$\|(g_{7/2}h_{11/2})\ 2,34\rangle$	0.205
$\|(d_{5/2}h_{11/2})\ 3,12\rangle$	−0.416	$\|(d_{5/2}h_{11/2})\ 6,00\rangle$	−0.398
$\|(d_{5/2}h_{11/2})\ 3,20\rangle$	0.215	$\|(s_{1/2}h_{11/2})\ 6,00\rangle$	−0.370
$\|(d_{5/2}h_{11/2})\ 4,12\rangle$	−0.334	$\|(d_{5/2}h_{11/2})\ 6,12\rangle$	0.234
$\|(d_{5/2}h_{11/2})\ 5,12\rangle$	−0.223	$\|(s_{1/2}h_{11/2})\ 6,12\rangle$	0.310
$\|(s_{1/2}h_{11/2})\ 5,12\rangle$	−0.202	$\|(d_{5/2}h_{11/2})\ 8,12\rangle$	0.372
		$\|(d_{5/2}h_{11/2})\ 8,22\rangle$	−0.239
8_1^-			
$\|(s_{1/2}h_{11/2})\ 6,12\rangle$	0.204	4_1^-	
$\|(d_{5/2}h_{11/2})\ 8,00\rangle$	−0.634	$\|(d_{5/2}h_{11/2})\ 3,12\rangle$	−0.396
$\|(d_{5/2}h_{11/2})\ 8,12\rangle$	0.554	$\|(d_{5/2}h_{11/2})\ 4,00\rangle$	−0.622
$\|(d_{5/2}h_{11/2})\ 8,20\rangle$	−0.203	$\|(d_{5/2}h_{11/2})\ 5,12\rangle$	0.211
$\|(d_{5/2}h_{11/2})\ 8,24\rangle$	−0.237	$\|(d_{5/2}h_{11/2})\ 6,12\rangle$	0.274
5_1^-		7_1^-	
$\|(d_{5/2}h_{11/2})\ 3,12\rangle$	−0.372	$\|(d_{5/2}h_{11/2})\ 5,12\rangle$	−0.266
$\|(d_{5/2}h_{11/2})\ 5,00\rangle$	0.407	$\|(s_{1/2}h_{11/2})\ 5,12\rangle$	−0.250
$\|(s_{1/2}h_{11/2})\ 5,00\rangle$	0.355	$\|(d_{5/2}h_{11/2})\ 7,00\rangle$	0.551
$\|(d_{5/2}h_{11/2})\ 5,12\rangle$	−0.208	$\|(d_{3/2}h_{11/2})\ 7,00\rangle$	−0.286
$\|(s_{1/2}h_{11/2})\ 5,12\rangle$	−0.313	$\|(d_{5/2}h_{11/2})\ 7,12\rangle$	−0.338
$\|(d_{5/2}h_{11/2})\ 7,12\rangle$	−0.214	$\|(d_{3/2}h_{11/2})\ 7,12\rangle$	0.279
10_1^-			
$\|(s_{1/2}h_{11/2})\ 6,24\rangle$	−0.258		
$\|(d_{5/2}h_{11/2})\ 8,12\rangle$	0.695		
$\|(d_{5/2}h_{11/2})\ 8,22\rangle$	−0.336		
$\|(d_{5/2}h_{11/2})\ 8,24\rangle$	−0.411		

Table VI- Wave functions of a few negative-parity model states. Only those components are listed which are larger than 4%.

tion theorem used here can be generalized to higher orders[57]. It is of the same type as the Bethe-Brandow-Petschek factorization theorem, giving rise to "on-energy-shell" insertions to hole lines in nuclear-matter calculations[47]. In the present situation, the effective charge for the crossover transition

$$e_{\mathrm{eff}}(2_2 \to 0,) = e^{\mathrm{s.p.}} + \frac{5}{\sqrt{\pi}}\, \mathbf{e}^{\mathrm{vib}}\, |a| \left[\frac{1}{\Delta + 2\hbar\omega} - \frac{1}{\mathbf{A}}\right]$$

is small, because the collective part involves interna1 incoherence. Furthermore, when $e^{\mathrm{s.p.}} > 0$, additional reduction results from the incoherence of single-particle and collective contributions to the effective charge.

The qualitative result for the reduction of the crossover transition is rather general, independent of the particular zeroth-order situation[39].

The general quasirotational feature of the cluster-field coupling scheme is the appearance of the ground-state quasirotational band. The calculation for ^{94}Mo clearly reproduces the $10_1^+ \to 8_1^+ \to 6_1^+ \to 4_1^+ \to 2_1^+ \to 0_1^+$ band, with strong E2 transitions inside the band and negative quadrupole moments of the members of the band, thus reflecting a kind of prolate deformation produced by the cluster-field mechanism[41]. In the present calculation higher-spin states are expected to be stretched and the corresponding B(E2) values overestimated because of the truncation of the phonon space and possible phase transitions.

We shall briefly describe the physical picture of the quadrupole moment of the first-excited state which is a one-phonon multiplet state in zeroth order. The leading-order contributions to the quadrupole moment come from second-order particle processes involving a single particle interacting with the electromagnetic field and from third-order induced collective processes with the absorption or emission of virtual phonons by the electromagnetic field. The corresponding diagrams are drawn in Fig. 3.

The factorization theorem mentioned previously can be applied to the four induced diagrams in each line. The induced collective terms again give rise to an effective charge taken "on the energy shell", i.e., the configuration-independent effective charge corresponding to the quadrupole moment of a single-particle state. This theorem also applies to higher-order processes[57]. The general result is illustrated in Fig. 4. Consequently, the quadrupole moment is given by the sum of all E2 contributions of the single-particle (cluster) type, while the induced E2 terms of the collective type are incorporated into the effective charge

$$e_{\mathrm{eff}}(2_1) = e^{\mathrm{s.p.}} + \frac{5}{\pi^{1/2}}\, e^{\mathrm{vib}} \,|a|\, \frac{1}{\hbar\omega},$$

which is independent of the shell-model configurations.

This gives rise to an appreciable enhancement of the cluster quadrupole moment.

In this way the quadrupole moment is essentially a shell effect resulting from the competition between the $Q\,|(j^2)2|$ diagonal and $Q\,|(j_1 j_2)2|$ < 0 ($j_1 = j_2 \pm 2$ or $j_1 = \frac{1}{2}, j_2 = \frac{3}{2}$) nonspin-flip off-diagonal contributions from the valence-shell clusters. This gives rise to a simple rule for the sign and magnitude of the quadrupole moment (GVISR)[39]. The same feature is also dominant in the structure of the quadrupole moment in the representation based on complete averaging over the shell structure[48].

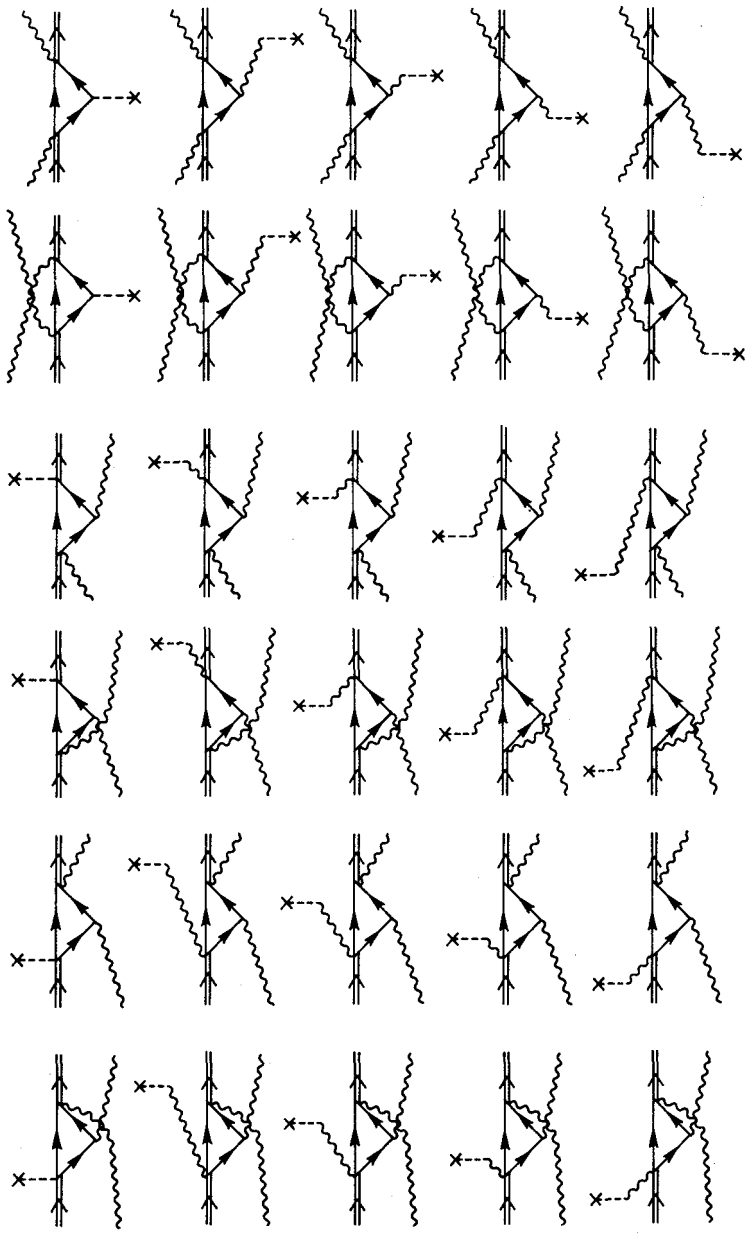

Fig. 3 - Second-order particle and third-order induced collective diagrams giving leading contributions to the quadrupole moment of the first excited state.

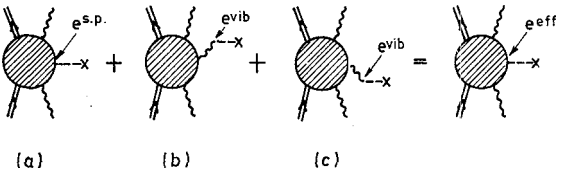

Fig. 4 - General structure of the quadrupole moment of the multiplet state. **A** set of induced collective diagrams 4b and 4c corresponds to each particle diagram 4a, giving rise to the effective charge. The points of phonon destruction (Fig. 4b) and creation by the electromagnetic field (Fig. 4c) may take on all possible time orderings.

The GVISR scheme in the case of ^{94}Mo is given in Table VII. The diagonal term in leading order giving a positive contribution to the quadrupole moment comes from the lowest available $(d_{5/2})^2 2$ two-neutron configuration, while the leading off-diagonal term contributing a negative part to the quadrupole moment is due to the $(d_{5/2}s_{1/2})2$ confíguration which is the only available nonspin-flip pair containing the lowest valence-shell single-particle state $d_{5/2}$. Thus, the quadrupole moment is a result of the competition between the positive (diagonal) and negative (offdiagonal) terms, with off-diagonal terms being predominant for experimental single-particle energies from Ref. 21. The quadrupole moment of ^{94}Mo is, therefore, very sensitive to details of calculation (parametrization and truncation), especially to the $s_{1/2}$ single-particle energy since it determines the magnitude of the dominant off-diagonal term. Table VIII illustrates this effect.

The sensitivity of the quadrupole moment in the so-called vibrational nuclei to certain shell-model confígurations is considered to be neither a virtue nor a shortcoming of the model. This pronounced shell effect is generally expected to be prcsent in any type of microscopic or semimicroscopic approach[50].

Heavier Te nuclei, where $g_{7/2}^2$ and $g_{7/2}d_{3/2}$ are the zeroth-order diagonal and the zeroth-order nonspin-flip off-diagonal terms, respectively, are classical examples of an unstable situation with off-diagonal terms being somewhat larger. Cancellation of the main terms leads to rather unstable negative quadrupole moments[39,40]. In Cd nuclei, the diagonal terms are dominant [$g_{9/2}^2$ is the only zeroth-order term]. The off-diagonal terms $p_{1/2}^{-1}p_{3/2}^{-1}$, $p_{1/2}^{-1}f_{5/2}^{-1}$ are admixed due to pairing, reducing somewhat the diagonal contribution. Therefore, the quadrupole moment is expected to be negative

	$d_{5/2}$	$g_{7/2}$	$s_{1/2}$	$d_{3/2}$	$h_{11/2}$
$d_{5/2}$	*		**		
$g_{7/2}$					
$s_{1/2}$	**				
$d_{3/2}$					
$h_{11/2}$					

Table VII- GVISK scheme for the quadrupole moment of the first excited state of ^{94}Mo. The 2_1^+ state is based on the basis state containing a $(d_{5/2})^2$ single-particle cluster. The zeroth--order diagonal term is denoted by * and the available nonspin-flip off-diagonal zeroth-order term by **. For particles the diagonal terms are always positive, and the nonspin--flip off-diagonai terms negative.

[generally, the diagonal term for a two-hole cluster is negative, while for a two-particle cluster it is positive], with the magnitude sensitive to the $p_{1/2}^{-1}$, $p_{3/2}^{-1}$, and $f_{5/2}^{-1}$ single-hole positions[34,39,40]. Nuclei exhibiting no competition between diagonal and off-diagonal terms are expected to have rather stable and, therefore, large quadrupole moments. Such examples are Hg [$s_{1/2}^{-1}d_{3/2}^{-1}$ is the main off-diagonal term] and Fe [$f_{7/2}^{-2}$ is the main diagonal term], which are therefore predicted to have large, rather stable positive and negative quadrupole moments, respectively[32,39,49].

The present calculation also reproduces the elements of the second band in the yrast region, the quasirotational character of which is less pronounced. Transitions between the first and the second band are rather weak, while transitions inside the second band are moderate or strong [for example, $6_2^+ \rightarrow 4_2^+$ and $8_2^+ \rightarrow 6_2^+$, respectively]. In the low-lying part of the spectrum, the quasirotational pattern breaks into the quasivibrational structure. The quadrupole moments of the members of the second band are also negative, indicating that this band does not correspond to the γ band or to the second-potential minimum[41].

The qualitative discussion can be generalized to higher-spin states in the yrast region[41]. The present calculation, however, is limited by the truncation of the configuration space. For higher-spin states, the correlations which have been neglected may also become more important and phase transitions might occur.

The experimental situation in ^{94}Mo confirms the existence of the $6_1^+ \rightarrow$ $\rightarrow 4_1^+ \rightarrow 2_1^+ \rightarrow 0_1^+$ band, but the existence of possible higher-spin members has not yet been clarified experimentally. The tentative $(10^\pm)$ state at 3.894 MeV and the $(8^\pm)$ state at 2.953 MeV are relatively low-lying. Furtherrnore, if the $(8^\pm) \rightarrow 6_1^+$ transition is of the E2 type, the retardation should be appreciable, while the experimental $(8^\pm) \rightarrow (6^\pm)$ (at 2.870 MeV) transition seems to be rather strong[12]. The experimental $(10^\pm)$ and $(8^\pm)$ states, therefore, do not seem to correspond to the 10_1^+ and 8_1^+ states in our model. It is not clear whether such states do exist but have not been populated in existing experiments, or the model band structure breaks down for higher spins.

There are two possible explanations for the observed $(10^\pm)$ and $(8^\pm)$ states. If the states are of positive parity, they should be based on explicit two-quasiproton excitations[12], which are not included in the present calculation. If they are of negative parity, they are based either on $(\pi g_{9/2})^3 (\pi p_{1/2})$ $(\nu d_{5/2})$ (Ref. 12) or on the $(d_{5/2} h_{11/2})$ two-neutron configuration[6,8]. Our calculation of negative-parity states indicates the possibility of the second explanation.

The present calculation predicts the lowesi group of negative-parity states to be based on the $(d_{5/2}, h_{11/2})\, 3^-, 4^-, 5^-, 6^-, 7^-, 8^-$ two-neutron clusters. If the 2.870- and 2.953-MeV states observecl in experiment are of negative parity, the predicted group of negative-parity states seems to be confirmed experimentally: the 3_1^-, (5_1^-), (6_1^-), (8_1^-), and (4_1^-) states lie in the energy range of about 400 keV, and the (7_1^-) state lies a few hundred keV higher. However, the ordering of the calculated states in the lower group differs somewhat from the experimental ordering. At about 1.5 MeV above the lowest 3^- negative-parity state, the calculation predicts the pronounced 10^- negative-parity state with a rather strong E2 transition to the 8^- state. This state might obviously correspond to the experimental $(10^\pm)$ state at 3.894 MeV, with a pronounced transition to the $(8^\pm)$ state at 2.953 MeV.

Calculations indicate that negative-parity states also exhibit a quasirotational feature. The electromagnetic properties reproduce the elements of two negative-parity in the particle-field system is the one which produces dominant collective effects in the E2 moments. An analogous type of interaction in the case of M1 transitions would also involve velocity-dependent potentials. Especially, in the case of *l*-forbidden transitions, these correlations may become important[51].

			Q (eb)	
	A	B	I	II
a	− 0.461	− 0.409	− 0.27	− 0.29
b	− 0.382	− 0.304	− 0.20	− 0.21
c	− 0.272	− 0.202	− 0.13	− 0.14
d	− 0.011	0.037	0.02	0.03
e	0.104	0.149	0.10	0.10
f	0.216	0.302	0.21	0.22

Table VIII - Dependence of the quadrupole moment on the position of the $s_{1/2}$ single-particle level.

In cases (a)-(e) the following energies of the $s_{1/2}$ single-particle state have been used (a) $\varepsilon(s_{1/2}) = 1.55$ MeV, (b) $\varepsilon(s_{1/2}) = 2$ MeV, (c) $\varepsilon(s_{1/2}) = 2.5$ MeV, (d) $\varepsilon(s_{1/2}) = 5$ MeV, (e) $s_{1/2}$ not included in the configuration space The other parameters are the same as used in Sec IV

In case (f), only the $d_{5/2}$ state has been included in the single-particle configuration space to illustrate the influence of the predominantly off-diagonal terms arising from other single-particle configurations

The strong incoherence between the collective and single-particle part is a characteristic neutron effect appearing in some M1 transitions in ^{94}Mo. Because of this incoherence the B(M1) values are more sensitive to parametrization and might provide evidence for renormalizations of the bare gyromagnetic ratios.

The coexistence of the quasirotational and quasivibrational pattern, established in the cluster-field system, seems to be in agreement with experiments. Further experimental studies are desirable to realize the extent and limits of the present concepts in actual situations.

6. Discussion of Transfer Reactions

In this Section, a qualitative discussion of transfer experiments is given in the framework of the cluster-field coupling model.

The $(5/2)^+$ ground state of ^{93}Mo is strongly excited in the ^{94}Mo(d, t)^{93}Mo transfer reaction[14,15]. Higher states in ^{93}Mo are appreciably less populated by this transfer reaction than by the corresponding (d, p) reactions[20,21]. The ground states of ^{93}Mo and of ^{94}Mo are based on the $|d_{5/2},00; 5/2\rangle$ bands with pronounced $9_1^- \rightarrow 7$; $\rightarrow 5_1^- \rightarrow 3$; and $10_1^- \rightarrow 8$; $\rightarrow 6$; transitions inside the band and with the same sign and similar magnitudes of the quadrupole moments. The quadrupole moments are rather large and negative, and generally increase with spin. However, for even-spin negative-parity states the band is strongly distorted. Of the remaining E2 transitions between negative-parity states, the $4; \rightarrow 3$; transition is rather strong, reflecting a kind of quasivibrational structure. The calculated $6; \rightarrow 5;$ transition is of the predominantly M1 type.

The negative-parity model states are expected to be appreciably populated by the ^{93}Mo(d, p) ^{94}Mo transfer reaction, because the corresponding processes are allowed [going through zeroth-order components]. In the ^{93}Nb(^{3}He, d) ^{94}Mo reaction these states are predicted to be populated by first-order processes proceeding through rather pronounced one-phonon components.

However, additional types of negative-parity states based on octupole phonons and explicit two-quasiproton configurations are also expected to exist in this energy region. These states, which are outside of the scope of the present calculation, may mix with negative-parity model states. Our results for negative-parity states are, therefore, less reliable than those for positive-parity levels.

In the present model, the description of the magnetic properties is expected to be poorer than that of the electric properties. The reason is that the interaction used and $|(d_{5/2})^2 0,00;0\rangle$ zeroth-order configurations, respectively. The ground state of ^{93}Mo is populated by zeroth-order processes in both (d, t) and (d, p) reactions. The states based on other single-particle states, namely $(1/2)^{\pm}$, $(3/2)^{\pm}$, and $(7/2)^{\pm}$, are populated by first-order pairing processes in the (d, t) reaction, whereas in the (d, p) reaction they are directly excited. The states based on single-particle multiplets are populated by higher-order processes, including particle-vibration coupling vertices. The (d, t) experiment provides evidence for the $(s_{1/2})^2 0$, $(d_{3/2})^2 0$, $(g_{7/2})^2 0$ seniority-zero admixtures in the ground state of ^{94}Mo, associated with pairing correlations. On the other hand, the low-lying $(9/2)^{\pm}$ state in ^{93}Mo reveals the presence of ground-state correlations [2 particle 1 hole state]. This is a phenomenon characteristic of the vicinity of closed shells[42,44]

In the ^{94}Mo(p, t) ^{92}Mo reaction, the ground state of ^{92}Mo is rather strongly excited, and the low-lying states of this nucleus are weakly populated[16,17]. This means that in a simple shell-model picture the ground state of ^{94}Mo contains configurations of higher seniority in addition to proton and neutron configurations of seniority zero[17]. In the present semimicroscopic model, the ground state of ^{94}Mo contains admixtures of $|12)$ one-phonon, $|20\rangle$, $|22\rangle$, and $|24)$ two-phonon states, etc. However, additional channels are also open because of the correlations neglected in this approach. The $(d_{5/2})^2 0$, $(s_{1/2})^2 0$, $(g_{7/2})^2 0$, $(d_{3/2})^2 0$, and $(h_{11/2})^2 0$ neutron pairs contribute coherently to the form factor for the $0_1^+ \rightarrow 0_1^+$ two-particle transfer. The main part comes from the basic configuration $(d_{5/2})^2 0$. The ratio of the $(s_{1/2})^2 0$ to the $(d_{5/2})^2 0$ strength obtained in our calculation (Table II) corresponds to the one (≈ 0.1) from the shell-model calculation in Ref. 16. In addition, we obtain weak contributions from the $(g_{7/2})^2 0$, $(d_{3/2})^2 0$, and $(h_{11/2})^2 0$ pairs which were neglected in the shell model calculation. The $0_1^+ \rightarrow 2_1^+$ (p, t) transfer in the present model follows mainly from one-phonon components in the ground state of ^{94}Mo with the $(d_{5/2})^2 2$, $(d_{5/2}s_{1/2})2$, and $(s_{1/2}d_{3/2})2$ broken neutron pairs.

At higher excitation energies, pairing phonons are expected to become a pronounced feature of the (p, t) and (t, p) excitation mechanism, especially for 0^+ states. They may appreciably mix with two-phonon states[52,42].

The ^{93}Nb(^{3}He, d) ^{94}Mo stripping reaction yields a pronounced experimental result: the lowest 2_1^+ state is more strongly excited than the second 2_2^+ state by one order of magnitude[1*]. This contradicts the existing shell-model calculations which take ^{88}Sr or ^{90}Zr as a core[22,23]. These calculations describe the 2_1^+ and 2_2^+ states as deriving most of their parentage from the $(2d_{5/2})^2 2$ neutron and $(1g_{9/2})^2 2$ proton group, respectively. The coupling of a transferred $g_{9/2}$ proton to an unpaired $g_{9/2}$ proton in the ground state of ^{93}Nb should then preferentially excite the second 2_2^+ rather than the first 2_1^+ state in ^{94}Mo. This result of the shell-model calculation is probably due not only to the restricted configuration space but also to the inadequate effective interaction [the zeroth-order situation has to be changed]. The present approach accounts naturally for the experimental situation. The ^{93}Nb ground state in zeroth-order arises from a $g_{9/2}$ quasiproton coupled to a $(d_{5/2})^2 0$ neutron pair. In this way, the ^{93}Nb(^{3}He, d) ^{94}Mo reaction mainly excites the $|(d_{5/2})^2 0, 12\rangle$ component through the $(g_{9/2})^2 2$ two-quasiproton configuration, creating a phonon by a first-order process. In our approach, the 2_1^+ and 2_2^+ states in ^{94}Mo arise from the $|(d_{5/2})^2 0, 12; 2\rangle$ and $|(d_{5/2})^2 2, 12; 2\rangle$ basic configurations, respectively. The pattern of the experimental proton transfer, therefore,

is qualitatively well understood. The basic component of the 2_1^+ state is populated by a first-order process (Fig 5) and that of the 2_2^+ state by third-order processes (Fig. 6). The 2_1^+ state in leading order is predicted to be more strongly excited than the 2_2^+ state by about 30 times. Higher order processes give rise to the excitation of zero- and two-phonon states and/or different valence-shell neutron configurations.

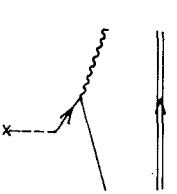

Fig. 5 - The leading process for populating the 2_1^+ state by the ^{93}Nb(^{3}He, d)^{94}Mo reaction.

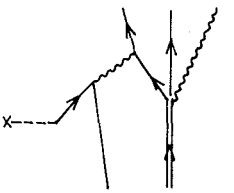

Fig. 6 - Illustration of the leading-order process for populating tlie 2_2^+ state by the ^{93}Nb(^{3}He, d)^{94}Mo reaction.

The ^{95}Mo (d, t) ^{94}Mo and ^{94}Mo (p, p′γ) reactions[19] give rise to an appreciable excitation of the 0_1^+, 2_1^+, and 4_1^+ states, the 4_1^+ states being more strongly excited than the 2_1^+ state. This experimental situation, considered in the framework of the present model, is a consequence of the character of the states involved. The 0_1^+ and 4_1^+ states are based on the $|(d_{5/2})^2 0,00;0\rangle$ and $|(d_{5/2})^2 4,00;4\rangle$ zero-phonon components, respectively, while the 2_1^+ state is based on the $|(d_{5/2})^2 0,12;2\rangle$ one-phonon component. The ground state of ^{95}Mo arises from the $|(d_{5/2})^3\ 5/2,00;5/2\rangle$ zero-phonon component. Consequently, the excitation in zeroth-order is allowed for the 0_1^+ and 4_1^+ states, while it is forbidden for the 2_1^+ state. First-order processes involving pairing vertices increase the population of the 0_1^+ state, and first-order particle-vibration coupling processes contribute to the excitation strength of the 2_1^+ state.

It should be mentioned that the present approach involves interferent effects in processes proceeding via isobaric analogue resonances. The usual type of analysis might be too rigid in the situations where a few-particle cluster appears in the valence shell. Results for the ^{94}Mo (p, p′γ) ^{94}Mo reaction are expressed in the usual way in terms of the relative c.f.p.s. of the $5/2^+$ ground state in ^{95}Mo for the configurations $|d_{5/2}, 2^+; 5/2\rangle$,

$|d_{3/2}, 2^+; 5/2\rangle$, $|d_{5/2}, 4^+; 5/2\rangle$, etc., where 2^+ and 4^+ are the first and second excited states of ^{94}Mo, respectively[19]. However, the process may also proceed between different components of the cluster-phonon system in both the initial and final states. This gives rise to interference effects, neglected in the usual type of analysis. This comment also applies to the analysis of the (d,t) transfer reaction.

A similar type of cluster-field competition is expected to play an important role also in inelastic scattering[33,53,54]. Theoretical approaches to inelastic scattering are usually based on either a collective or a microscopic description of nuclear states. In the framework of the cluster-field model, inelastic scattering is an interferent scattering process in collective and single-particle cluster channels.

7. Shell-Model, Single Particle Cluster — Vibration, or Single-Particle Cluster — Rotation Coupling Model?

The above three approaches can be used in microscopic or semimicroscopic theoretical attempts to understand odd and even nuclei in the spherical and transitional regions. It is obvious that the same physical phenomena are described by different representations.

Shell-model calculations could, in principle, give the proper description, provided the full space of all active configurations contributing noticeably to the properties of the nuclear system is taken into account. However, this goal usually lies out of reach of computing possibilities. One is, therefore, forced to truncate the space rather severely, which leads to a loss in amount of physical information.

Alternative approaches are based on describing the nuclear system in terms of collective variables obtained by averaging over the shell-model structure. Such approaches are applied when the averaging is expected to be a fair representation of the actual situation, and have been successfully used in a number of transitional nuclei[26,27,59].

Additional explicit shell effects could then be included by coupling the dominant valence-shell few-particle clusters to the collective field. This method allows to account for a much larger effective space than in the corresponding shell-model calculations. The two simple choices of the basic representations are as follows:

(i) Spherical representation, *i.e.*, coupling of single particles in shell-model spherical configurations to vibrations;

(ii) Deformed representation, *i.e.*, coupling of single particles in Nilsson orbitals to rotations.

Both representations can be used to describe an intermediate physical situation in spherical'and transitional nuclei, which is characterized by the coexistenceof the quasirotational and quasivibrational pattern[41,45,53,56]. The cluster-field interaction introduces quasirotational elements into (i), while the Coriolis coupling introduces quasivibrational elements into (ii).

7. Interpretation of Model Predictions

Correlations taken into account in the present approach lead to a type of quasivibrational, quasirotational, and clustering structure, but leave a certain degree of flexibility in quantitative predictions.

A certain amount of data available roughly determine the parametrization [single-particle positions, phonon energy, zero-point amplitude, and gyromagnetic ratios]. On the other hand, one should be aware of renormalization effects on propagators and vertices associated with the truncation of the configuration space, isovector potential, bare residual Q-Q force, etc. Consequently, a certain degree of freedom remains in the parametrization in actual calculations.

In addition, types of residual interactions and coupling to higher modes which cannot be included in renormalizations, Yelocitydependent terms in operators, etc., would introduce additional correlations, partly changing results or giving rise to new phenomena.

For these reasons one should not take the quantitative results of the cluster--field coupling model too rigidly. Specifically, quantities based on large interna1 incoherence are unstable and, therefore, the choice of parametrization and the correlations which have been neglected in this calculation, might appreciably influence the quantitative results. On the other hand, the model exhibits definite qualitative features, reflecting the basic under-

lying cluster and multiplet structure and generalized vibrational selection and intensity rules (GVISR)[39].

The pronounced qualitative (coexistence) and, to some extent, also quantitative successreflects the irnportance of physical correlations accounted for in the present type of approach. However, quantitative results should be considered within the framework of limitations discussed in this Section. In such a situation, fitting of parameters and optimization have not been attempted.

The author would like to express his gratitude to Professor G. Alaga for initiating and stimulating this work and for many ideas and explanations conceming the physical background. Sincere thanks are due to Professors D. Bès, K. Kumar, B. Mottelson, Dr. B. Sorensen, and Dr. V. Lopac for helpful discussions, and to Dr. J. Barette for correspondence. The autor is indebted to the Niels Bohr Institute for excellent working conditions.

References

1. G. M. Temmer and N. P. Heydenburg, Phys. Rev. 104, 967 (1956).
2. P. H. Stelson and F. K. McGowan, Phys. Rev. 110, 489 (1958).
3. Yu. P. Gangrskii and I. Kh. Lemberg, Izv. Akad. Nauk SSSR (ser. fiz.) 26,1001 (1962).
4. S. Monaro, G. B. Vingiani, R. A. Ricci and R. van Lieshou, Physica 28, 63 (1962).
5. J. M. Matuszek and T. T. Sugihara, Nucl. Phys. 42,582 (1963); J. H. Hamilton, K. E. G. Lobner, A. R. Sattler, and R. van Lieshout, Physica 30, 1802 (1964); K. A. Baskova, S. S. Vasilev, M. A. Khamo-Leila and L. Y. Shovtvolov, Izv. Akad. Nauk SSSR (ser.fiz.) 29,2255 (1965).
6. N. K. Aras, E. Eichler, and G. G. Chilosi, Nucl. Phys. **A112,** 609 (1968).
7. J. Barette, A. Boutard, and S. Monaro, Can. J. Phys. 47, 995 (1969).
8. Y. S. Kim and B. L. Cohen, Phys. Rev. 142, 788 (1966).
9. H. F. Lutz, D. W. Heikkinen, and W. Bartolini, Phys. Rev. C4, 934 (1971).
10. P. J. Riley, J. L. Horton, C. L. Hollas, S. A. A. Zaidi, C. ,M. Jones, and J. L. C. Ford, Jr., Phys. Rev. C4, 1864 (1971)
11. J. M. Jaklevic, C. M. Lederer, and J. M. Hollander, UCRL 19530 (1970).
12. C. M. Lederer, J. M. Jaklevic, and J. M. Hollander, Nucl. Phys. A169 (1971) 449.
13. J. Delaunay-Olkowsky, P. Strohal, and N. Cindro, Nucl. Phys. 47, 226 (1963).
14. H. Ohnuma and J. L. Yntema, Phys. Rev. **178,** 1855 (1969).
15. R. C. Diehl, B. L. Cohen, R. A. Moyer, and L. ti. Goldman, Phys. Rev. C1, 2132 (1970).
16. A. Moalem, M. A. Moinester, N. Auerbach, J. Alster, and Y. Dupont, Nucl. Phys. **A177,** 145 (1971).
17. H. Taketani, M. Adachi, M. Ogawa, K. Ashibe and T. Hattori, Phys. Rev. Letters 27, 520 (1971).
18. M. R. Cates, J. B. Ball, and E. Newman, Phys. Rev. 187. 1682 (1969).
19. E. Abramson, G. Engler, Z. Vager, N. Cue, I. Plesser, and G. F. Wheeler, Phys. Letters **38B** 70 (1972).
20. S. A. Hjorth and B. L. Cohen, Phys. Rev. **135B,** 920 (1964).
21. J. B. Moorhead and R. A. Moyer, Phys. Rev. 1184, 1205 (1969).
22. K. H. Bhatt and J. B. Ball, Nucl. Phys. **63,** 286 (1965).
23. J. Vervier, Nucl. Phys. 75, 17 (1966).
24. L. K. Peker, Proc. of the Winter School for Nuclear Theory and High-Energy Physics, Physical-Technical Institute, Leningrad, part I (1969) p. 163.
25. N. Auerbach and I. Talmi, Nucl. Phys. **64,** 453 (1965).
26. A. S. Davydov and A. A. Chaban, Nucl. Phys 20, 499 (1960).
27. A. Bohr and B. R. Mottelson, Mat. Fys. Medd. Dan. Vid. Selsk. 27, No. 16 (1953).
28. A. Bohr and B. R. Mottelson, Nuclear *Structure*, Vol. II, to be published.
29. D. C. Choudhury, Mat. Fys. Medd. Dan. Vid. Selsk. 28, No. 4 (1954).
30. B. J. Raz, Phys. Rev. 114, 1116 (1959).
31. G. Alaga, Bull. Am. Phys. Soc. 4, 359 (1959).
32. G. Alaga and G. Ialongo, Phys. Letters 22,619 (1966); G. Ialongo, Thesis, New York University, 1966.
33. G. Alaga, Rendiconti Scuola Internazionale di Fisica "E. Fermi", Varenna, XL Corso, 28 (1967); G. Alaga, *Cargèse* lectures *in* physics, Vol. 3 (Gordon and Breach, 1969), p. 579.
34. G. Alaga, F. Krmpotic, and V. Lopac, Phys. Letters 24B 537 (1967).
35. A. Covello and G. Sartoris, Nucl. Phys. **A104** (1967) 189.
36. K. Heyde and P. J. Brussaard, Nucl. Phys. **A104,** 81 (1967).
37. D. R. Bès and G. G. Dussel, Nucl. Phys **A135,** 1 (1969).
38. V. Lopac, Nucl. Phys. **A155,** 513 (1970).

39. G. Alaga, V. Paar, and V. Lopac, Phys. Letters **43B,** 459 (1973); G. Alaga, F. Krmpotic, V. Lopac, V. Paar, and L. Sips, to be published.
40. V. Lopac, Thesis, University of Zagreb, 1971.
41. G. Alaga and V. Paar, to be published.
42. R. A. Broglia, V. Paar, and D. R. Bes, Phys. Letters **37B,** 159 (1971); Phys. Letters **37B,** 257 (1971), and to be published.
43. V. Paar, Nucl. Phys. **A164,** 576 (1971), **A164,** 593, (1971), and **A166,** 341 (1971).
44. D. R. Bès and R. A. Broglia, Phys. Rev. **C3,** 2349 (1971) and Phys. Rev. **C3,** 1619 (1971).
45. V. Paar, Phys. Letters 39B, 466 (1972), **39B,** 587 (1972), **42B,** 8 (1972), and to be published.
46. L. S. Kisslinger and R. A. Sorensen, Rev. Mod. Phys. **35** 853 (1963).
47. H. A. Bethe, B. H. Brandow, and A. G. Petschek, Phys. Rev. 129,225 (1963).
48. R. Broglia, R. Liotta, and V. Paar, Phys. Letters 38B 480 (1972) and to be published.
49. V. Paar, Nucl. Phys. **A185,** 544 (1972).
50. G. Alaga, V. Paar, R. Broglia, R. Liotta, and V. Lopac, to be published.
51. S. de Barros, M. J. Bechara, T. Borello-Lewin, and V. Paar, Preprint, ICTP, IC/73/172 and to be published.
52. B. Sorensen, private cornmunication.
53. G. Alaga, private communication.
54. J. L. De Jager and E. Boeker, Nucl. Phys. **A186,** 393 (1972).
55. R. Broglia, B. Nilsson, and V. Paar, to be published.
56. B. Mottelson, private communication.
57. V. Paar, Preprint JINR and to be published.
58. J. Barette, M. Barette, A. Boutard, R. Haroutunian, G. Lamoureux, and S. Monaro, Phys. Rev. **C6,** 1339 (1972).
59. K. Kumar and B. Baranger, Nucl. Phys. 62,113 (1965), **A92,** 608 (1967), **A110,** 490 and 529 (1968).